The following publication X. W. Zhao et al., "Modulating Antiferromagnetic La0.35Sr0.65 MnO3 via Low-Voltage Pulsing Across a Ferroelectric Copolymer Gate Dielectric," in IEEE Transactions on Magnetics, vol. 58, no. 2, pp. 1-5, Feb. 2022, Art no. 4200205 is available at https://doi.org/10.1109/TMAG.2021.3085364

Modulating Antiferromagnetic $La_{0.35}Sr_{0.65}MnO_3$ via Low-Voltage Pulsing across a Ferroelectric Copolymer Gate Dielectric

Xu Wen ZHAO[1], Hon Fai WONG[1], Yu Kuai LIU[1,2], Sheung Mei NG[1], Jing Ming LIANG[1], Ka Kin LAM[1], Wang Fai CHENG[1], Chee Leung MAK[1], Chi Wah LEUNG[1*]

[1]Department of Applied Physics, The Hong Kong Polytechnic University, Hung Hom, Hong Kong, China
[2]College of Electronic Information and Mechatronic Engineering, Zhaoqing University, Zhaoqing 526061, Guangdong, China

Electric-field based modulation is a promising way for realizing ultrafast and high density antiferromagnetic spintronics. Here, we investigate low-voltage-pulse modulation of antiferromagnetic $La_{1-x}Sr_xMnO_3$ (x = 0.65) (AF-LSMO) thin films. Positive voltage pulses can increase the resistance at low temperatures, which is ascribed to the oxygen vacancies induced by positive voltage pulses. This effect is supported by x-ray photoelectron spectra (XPS) results. Using low-voltage pulses, we demonstrate exchange bias modulation in ferromagnetic $La_{0.7}Sr_{0.3}MnO_3$ (FM-LSMO)/AF-LSMO bilayer structure. Both temperature-dependent resistance, exchange bias field and coercivity show voltage-polarity dependence. While positive pulses can induce significant changes in the AF-LSMO, negative pulsing has little impact and is consistent with oxygen vacancy related process observed in various electrochemical reaction systems. Our findings can find potential for exploring electric-field modification of antiferromagnetic spintronics.

Index Terms—**Antiferromagnetism, AF-LSMO thin film, ferroelectric copolymer, low-voltage pulses.**

I. Introduction

Perovskite oxides have been widely investigated due to the strong correlation between spin, charge, orbital and lattice degrees of freedom [1]-[3]. For example, ferromagnetic manganites $La_{1-x}Sr_xMnO_3$ (LSMO) with optimal doping (x = 0.33) has been deployed in spin valves [4], field effect transistors [5], and tunnel junctions [6]. However, studies on the antiferromagnetic counterparts in the LSMO system with high Sr doping is limited due to larger tolerance factor, which makes the structure relatively unstable [7], [8]. Deposition of high-quality epitaxial films is an alternative approach to study the physical property of $La_{1-x}Sr_xMnO_3$ with $x > 0.5$ [8]-[10].

Antiferromagnetic materials have potential for magnetic device applications since they are insensitive to external perturbations [11], [17]. Regulation of antiferromagnets has been realized by strain effect [18], electrical methods (either via electrical current or electric field) [11], [19], [20], magnetic control [21] and optical modulation [22]. Among these, electric field control is promising due to the low operation energy [20], [23]. For example, electric field control of multiferroelectric $BiFeO_3$ and Cr_2O_3 via magnetoelectric coupling [24], [25], ferroelectric field effect modulation of Mn_2Au [20], NiO [26] and FeRh [23], and ionic liquid modulation of IrMn [27].

Manipulation of antiferromagnetism by ferroelectric copolymer of polyvinylidene fluoride with trifluoroethylene [P(VDF-TrFE)] has not been reported. P(VDF-TrFE) is widely used in organic and inorganic field effect transistors due to its low coercivity (1 MV/cm), high remnant polarization (10 μC/cm^2), and ease of processing [28]-[30]. Using P(VDF-TrFE) copolymer to regulate antiferromagnetism could provide a new route for flexible antiferromagnetic spintronic devices.

Here, we deploy P(VDF-TrFE) as the top gate dielectric for nonvolatile control of electrical and magnetic properties of epitaxial antiferromagnetic $La_{0.35}Sr_{0.65}MnO_3$ (AF-LSMO) thin films. A low-voltage pulsing scheme was used to control the physical properties of AF-LSMO thin films, by applying pulses with voltage lower than ferroelectric switching threshold [31], [32]. In such a manner, the electrical breakdown of the dielectric layer can be suppressed. On the other hand, small electric field can contribute no charge accumulation/depletion at the interface, which would imply mechanisms other than electrostatic charging effect.

To probe the magnetic properties of AF-LSMO, we prepared a 5-nm FM-LSMO layer underneath the AF-LSMO; it permits coherent growth of AF-LSMO on top due to literally identical lattice parameters, and at the same time serves to examine the AF-LSMO layer by exchange bias effect [33], [34]. By considering the electrical properties of the films, X-ray photoemission spectroscopy (XPS), and resistance vs. temperature (R-T) plots and magnetoresistance (MR) curves, we attribute the modulation of AF-LSMO to the creation/annihilation oxygen vacancies during the pulsing process.

II. Experimental Details

Epitaxial AF-LSMO and FM-LSMO thin films were grown on TiO_2-terminated $SrTiO_3$ (001) (STO) substrates by pulsed laser deposition (PLD), using excimer KrF laser (wavelength 248 nm) to ablate the corresponding ceramic targets at a frequency of 1 Hz; TiO_2-terminated STO substrates were prepared through leaching in boiling deionized (DI) water and thermal annealing processes [31], [32]. FM-LSMO layers were deposited in an oxygen pressure of 150 mTorr and substrate temperature of 700^0 C, which were then post-annealed at 10 Torr oxygen for 5 minutes at the same

Manuscript received ***; revised *** and ***; accepted ***. Date of publication ***; date of current version ***.

Corresponding author: Chi Wah LEUNG (e-mail: dennis.leung@polyu.edu.hk).

temperature. For AF-LSMO films, they were deposited in 150 mTorr oxygen pressure at 600 ^{0} C, along with 5-mintue post-annealing in 10 Torr oxygen at 600^0 C to reduce oxygen vacancies in as-grown samples.

Hall bar devices were prepared from as-deposited films, first by defining the patterns via photolithography (channel size 50 μm×100 μm) and then chemical etching in KI solution to remove the exposed parts of films [35]. Contact pads of Ti(5 nm)/Au(50 nm) were prepared by sputter deposition. Finally, 250-nm P(VDF-TrFE) was prepared as the top gate dielectric, covered on top by 100-nm Al gate electrode by electron beam evaporation through a shadow mask.

Transport properties of devices were measured in the patterned devices, firstly in pristine state, followed by positive pulsing state and finally negative pulsing. All the low-voltage pulses were applied in vacuum at 300 K. R-T plots and MR measurements were conducted with a constant current of 1 μA at the end of each state. For MR measurements, ±5k Oe magnetic field was applied during cooling from 300 K to 20 K to establish the exchange bias effect. 10 training cycles were conducted to eliminate training effect [36].

All the XPS spectra were measured by a Thermo Fisher Nexsa X-ray Photoelectron Spectrometer system with a monochromatic Al source (Kα = 1486.7 eV). The binding energy was calibrated to the C 1s spectrum (248.8 eV).

III. Results and Discussions

Before investigating the low-voltage pulsing effect on AF-LSMO, crystallinity and surface morphology of 7-nm AF-LSMO were characterized by x-ray diffraction (XRD) and atomic force microscopy (AFM). Fig. 1(a) shows the $\theta/2\theta$ scan of a 7-nm AF-LSMO film, with a broadened peak due to reduced thickness. As a comparison, relative thick (15 nm) AF-LSMO shows clear Laue fringes, indicating high quality of the AF-LSMO thin films. The strong texture with low mosaic spread of 7-nm AF-LSMO is confirmed by the narrow ω-scan peak (full-width at half-maximum, FWHM, ~ 0.1º) (inset of Fig. 1(a)). Fig. 1(b) shows the AFM image of the 7-nm AF-LSMO thin film with root-mean-square roughness of 0.25 nm, indicating atomically flat surface.

Few studies about antiferromagnetic LSMO (x > 0.5) thin films have shown the connection between R-T plots and the magnetic properties [8], [9]. Therefore, low-voltage regulation of 7-nm AF-LSMO on its R-T behaviour was investigated. The device schematic is shown on top panel of Fig. 1(c). The bottom panel of Fig. 1(c) displays the pulsing protocol; measurements were made at the end of each stage. Fig. 1(d) plots the R-T variation of 7-nm AF-LSMO thin film at pristine state, stage I, and stage II. Three regions are identificed in the R-T plot: Above 250 K, the increased resistance with reducing temperature is associated with the paramagnetic-to-antiferromagnetic phase transition [37]. At intermediate temperatures (between 100 K and 250 K) the R-T plot reaches a plateau, and it is possibly associated with the mixed spin structures or short-range magnetic ordering in the thin AF-LSMO, which was previously reported in heavily-doped bulk or ultrathin AF-LSMO films [8], [9], [37], [38]. For ideal A-type AF insulators, the magnetic spins are ferromagnetically aligned in plane (*ab* plane) while antiferromagnetically aligned out of plane (along *c* axis). For AF-LSMO, due to the chemical disorders, local ferromagnetic ordering could appear with decreasing temperatures. As is known, tensile strain prefers in-plane d_{x2-y2} orbital occupation while compressive strain promotes out-of-plane d_{3z2-r2} orbital filling [39]. Due to the in-plane tensile strain in 7-nm AF-LSMO, in-plane d_{x2-y2} orbital is preferred, along with enhanced ferromagnetic ordering. In the low temperature region (below 100 K), the resistance increases sharply again, suggesting the presence of an antiferromagnetic spin structure at low temperatures.

RT of the sample at stage I shows virtually no change from the pristine state in the high temperature range. In the intermediate temperature range the sample has a resistance that deviating from the pristine state by up to 12% state. Finally, sample at stage II only shows minimal resistance change at the lowest temperatures compared with stage I, and the R-T behavior is virtually unchanged in intermediate and high temperature regimes.

A possible explanation of the R-T variation is the generation or annihilation of oxygen vacancies in the film. XPS measurement was used to evaluate the effect by probing the changes in Mn oxidation state of 7-nm AF-LSMO thin films. Note that XPS measurement was conducted after removing the copolymer and the gate electrode. The core-level spectra of Mn 2p are shown in Fig. 2(a). The peak positions of Mn $2p_{3/2}$ for pristine, stage I and stage II are shown in Table I. The small shift of binding energy by 0.3 ± 0.1 eV between stage I and stage II suggests the change of $Mn^{4+}/(Mn^{4+}+Mn^{3+})$ ratio during pulsing process.

To extract more information, Mn 2p spectra are fitted using the Avantage software [40], with a standard Shirley background being used. All the Mn 2p spectra are fitted by Mn^{3+} and Mn^{4+} components with Mn $2p_{3/2}$ locating at 640.8 eV and 642.25 eV, respectively [41], [42]. The $Mn^{4+}/(Mn^{4+}+Mn^{3+})$ ratio for pristine sample is (64.2 ± 2.3) % (in Table I), which is in good agreement with stoichiometric ratio in $La_{0.35}Sr_{0.65}MnO_3$ target. For sample at stage I, the ratio slightly decreases to (62.64 ± 1.8) %, indicating the reduced oxidation state of Mn element. For sample at stage II, the ratio increases to (75.02 ± 2.9) %. The variation of $Mn^{4+}/(Mn^{4+}+Mn^{3+})$ ratio suggests the formation/annihilation of oxygen vacancy during the pulsing process.

As a direct indicator of oxygen loss, the O 1s core-level spectra is also analyzed (Fig. 2(b)). Due to surface contamination, usually three components are considered: negatively charged lattice oxygen (OI), oxygen vacancy related component (OII) and component of chemisorption of carbonate or hydroxyl species (OIII) [43]. The peak positions of OI, OII and OIII locate at 528.55 eV, 531.1 eV, and 531.83 eV, respectively, very close to previous reports [43]. From Table I, we can see that +10V pulses increase the OII contribution while -10 V pulses suppresses it. This can also be

reflected by comparing the OI component between samples at stage I and stage II.

From the R-T and XPS results we can correlate the low-voltage pulses to the oxygen vacancy formation/annihilation in AF-LSMO thin films. The strong spin-lattice correlation in LSMO would therefore suggest that electrochemical process can modulate the magnetism of AF-LSMO. However, it is difficult to probe the magnetic properties of antiferromagnets directly. Alternatively, the exchange bias method was deployed by preparing a 5-nm FM-LSMO layer underneath a 15-nm AF-LSMO thin film. Thinner AF-LSMO layers were attempted but proved incapable to pin the bottom FM-LSMO layer.

Transport measurements of the FM-LSMO/AF-LSMO samples were measured in Hall bar geometries (Fig. 1(c)), with the magnetic field applied parallel to the sample surface along the current direction. Fig. 3(a) displays the R-T plot of the bilayer structure. A clear metal-insulator transition at 273 K can be seen, indicating the resistance at low temperatures is dominated by the bottom FM-LSMO layer.

To confirm the existence of exchange bias effect, MR [MR = $(R_{(H)}-R_{(0)})/R_{(0)}$] curves of pristine sample were measured at 20 K after field cooling (FC) in +5k Oe and -5k Oe (Fig. 3(b)). Here, we define H_{CL} as the MR peak position in the negative magnetic field and H_{CR} as the MR peak position in the positive magnetic field. The exchange bias field (H_{EB}) and coercivity (H_C) can be calculated by $H_{EB} = (H_{CR} + H_{CL})/2$ and $H_C = (H_{CR} - H_{CL})/2$. Cooling the sample in a positive field results in a negative shift of the MR and vice versa, which is consistent with the conventional negative exchange bias effect [44]. On the other hand, the MR curves show a more significant asymmetric behavior compared with our previous work using magnetometry [45]. This asymmetric behavior is a very common phenomenon in exchange bias system due to the coherent rotation and domain wall propagation during two directional magnetic field sweeping [46], [47].

While our goal is to modulate the magnetic property of AF-LSMO thin film, any change in the bottom FM-LSMO layer may complicate the interpretation of results. We have previously demonstrated that pulse modulation of FM-LSMO [31, 32] can alter its resistance, MR value at high field and Curie temperature (T_C). The RT curves of pristine state, stage I and stage II are shown in Fig. 4(a); note that for stage II of bilayer sample, 1.15 million pulses were applied, considering the asymmetric pulsing behavior on R-T plots of 7-nm AF-LSMO thin film as well as increased thickness of the top AF-LSMO layer. Despite the increased pulse number, the low-temperature resistance, MR value at high field and T_C show negligible change, suggesting the voltage-pulse effect has minimal impact on the bottom FM-LSMO layer.

The 20-K MR curves for pristine, stage I and stage II are plotted as the inset of Fig. 4(a). The extracted H_{EB} and H_C are shown in Fig. 4(b). The positive pulses can reduce the H_C and suppress the H_{EB}, while the negative pulses can only slightly reverse them back. To confirm the validity of this voltage-pulse effect on H_C and H_{EB}, more data points (solid black) with smaller step are shown in Fig. 4(b). This observation strongly suggests that low-voltage pulses can change the magnetic property of AF-LSMO thin film.

The pulse effect on the magnetic properties of AF-LSMO could be understood by two possible mechanisms. Firstly, as demonstrated by XPS data, oxygen vacancy creation (annihilation) could reduce (increase) the $Mn^{4+}/(Mn^{4+}+Mn^{3+})$ ratio in AF-LSMO, thus suppressing (enhancing) the superexchange-dominated antiferromagnetism in AF-LSMO and leading to the decrease (increase) of H_{EB} and H_C.

Another factor is lattice distortion or spin disorder caused by oxygen vacancies. A simple illustration is shown in Fig. 4(c). For the pristine state, both the FM-LSMO and AF-LSMO spins are well-ordered after establishing the exchange bias effect. For stage I, some oxygen ions are randomly driven out of the top AF-LSMO layer, leaving oxygen vacancies in the lattice structure. After establishing exchange bias effect, these lattice defects may lead to local spin disorders in the top AF-LSMO layer, thus suppressing the pinning effect and reducing the H_{EB} and H_C. While for stage II, only part of these spin disorder can be recovered. The detailed mechanism using low-voltage pulses to tune exchange bias effect in FM-LSMO/AF-LSMO structure need to be further studied.

IV. Conclusion

In summary, high-quality epitaxial AF-LSMO thin films were grown by PLD method. Both the electrical transport and magnetic properties of AF-LSMO thin films can be controlled by low-voltage pulses in field effect devices with ferroelectric P(VDF-TrFE) copolymer as the dielectric. By analyzing the low-voltage pulse effect on XPS results, oxygen vacancy creation/annihilation in AF-LSMO thin films are confirmed to result from the low-voltage pulses. This work would pave a new way for exploring electric field control of antiferromagnetic spintronics.

Acknowledgment

Support by the Hong Kong RGC (PolyU 153027/17P) and PolyU (1-ZE25, 1-ZVGH) are acknowledged.

References

[1] Y. Tokura and N. Nagaosa, "Orbital physics in transition-metal oxides," Science, vol. 288, pp. 462-467, 2000.

[2] E. Dagotto, "When oxides meet face to face," Science, vol. 318, pp. 1076-1077, 2007.

[3] F. Hellman et al., "Interface-induced phenomena in magnetism," Rev. Mod. Phys., vol. 89, p. 025006, 2017.

[4] F. J. Wang, C. G. Yang, Z. V. Vardeny, and X. G. Li, "Spin response in organic spin valves based on $La_{2/3}Sr_{1/3}MnO_3$ electrodes," Phys. Rev. B, vol. 75, no. 24, 2007.

[5] D. Preziosi, M. Alexe, D. Hesse, and M. Salluzzo, "Electric-field control of the orbital occupancy and magnetic moment of a transition-metal oxide," Phys. Rev. Lett., vol. 115, no. 15, p. 157401, Oct 9 2015.

[6] D. Pantel, S. Goetze, D. Hesse, and M. Alexe, "Reversible electrical switching of spin polarization in multiferroic tunnel junctions," Nat. Mater., vol. 11, no. 4, pp. 289-93, Feb 26 2012.

[7] M. Izumi, T. Manako, Y. Konishi, M. Kawasaki, and Y. Tokura, "$La_{1-x}Sr_xMnO_3$ superlattices composed of ferromagnetic x = 0.4 and antiferromagnetic x = 0.55 layers," Phys. Rev. B, vol. 61, pp. 12187-12195, 2000.

[8] A. Bhattacharya, X. Zhai, M. Warusawithana, J. N. Eckstein, and S. D. Bader, "Signatures of enhanced ordering temperatures in digital

superlattices of $(LaMnO_3)_m$ / $(SrMnO_3)_{2m}$," Appl. Phys. lett., vol. 90, no. 22, 2007.
[9] A. T. Wong et al., "Strain driven anisotropic magnetoresistance in antiferromagnetic $La_{0.4}Sr_{0.6}MnO_3$," Appl. Phys. lett., vol. 105, no. 5, p. 052401, 2014.
[10] S. J. May et al., "Enhanced ordering temperatures in antiferromagnetic manganite superlattices," Nat. Mater., vol. 8, no. 11, pp. 892-7, Nov 2009.
[11] P. Wadley et al., "Electrical switching of an antiferromagnet," Science, vol. 351, pp. 587-590, 2016.
[12] T. Jungwirth, X. Marti, P. Wadley, and J. Wunderlich, "Antiferromagnetic spintronics," Nat Nanotechnol, vol. 11, no. 3, pp. 231-41, Mar 2016.
[13] R. A. Duine, K. J. Lee, S. S. P. Parkin, and M. D. Stiles, "Synthetic antiferromagnetic spintronics," Nat. Phys., vol. 14, no. 3, pp. 217-219, Mar 2018.
[14] O. Gomonay, V. Baltz, A. Brataas, and Y. Tserkovnyak, "Antiferromagnetic spin textures and dynamics," Nat. Phys., vol. 14, pp. 213–216, 2018.
[15] L. Šmejkal, Y. Mokrousov, B. Yan, and A. H. MacDonald, "Topological antiferromagnetic spintronics," Nat. Phys., vol. 14, pp. 242-251, 2018.
[16] Y.-J. Hao et al., "Gapless surface Dirac cone in antiferromagnetic topological insulator $MnBi_2Te_4$," Phys. Rev. X, vol. 9, no. 4, 2019.
[17] R. Duine, "Spintronics: An alternating alternative," Nat. Mater., vol. 10, no. 5, pp. 344-5, May 2011.
[18] A. A. Sapozhnik et al., "Manipulation of antiferromagnetic domain distribution in Mn_2Au by ultrahigh magnetic fields and by strain," Phys. Status Solidi RRL, vol. 11, no. 4, 2017.
[19] H. Tsai et al., "Electrical manipulation of a topological antiferromagnetic state," Nature, vol. 580, no. 7805, pp. 608-613, Apr 2020.
[20] X. Chen et al., "Electric field control of Neel spin-orbit torque in an antiferromagnet," Nat. Mater., vol. 18, no. 9, pp. 931-935, Sep 2019.
[21] B. G. Park et al., "A spin-valve-like magnetoresistance of an antiferromagnet-based tunnel junction," Nat. Mater., vol. 10, no. 5, pp. 347-51, May 2011.
[22] S. Manz et al., "Reversible optical switching of antiferromagnetism in $TbMnO_3$," Nat. Photonics, vol. 10, no. 10, pp. 653-656, 2016.
[23] Z. Feng, H. Yan, and Z. Liu, "Electric-field control of magnetic order: from FeRh to topological antiferromagnetic spintronics," Adv. Electron. Mater., vol. 5, no. 1, 2019.
[24] A. Haykal et al., "Antiferromagnetic textures in $BiFeO_3$ controlled by strain and electric field," Nat. Commun., vol. 11, no. 1, p. 1704, Apr 6 2020.
[25] X. He et al., "Robust isothermal electric control of exchange bias at room temperature," Nat. Mater., vol. 9, no. 7, pp. 579-85, July 2010.
[26] Y.-J. Zhang, J.-H. Chen, L.-L. Li, J. Ma, C.-W. Nan, and Y.-H. Lin, "Ferroelectric strain modulation of antiferromagnetic moments in Ni/NiO ferromagnet/antiferromagnet heterostructures," Phys. Rev. B, vol. 95, no. 17, 2017.
[27] Y. Wang et al., "Electrical control of the exchange spring in antiferromagnetic metals," Adv. Mater., vol. 27, no. 20, pp. 3196-201, May 27 2015.
[28] R. C. G. Naber, B. de Boer, P. W. M. Blom, and D. M. de Leeuw, "Low-voltage polymer field-effect transistors for nonvolatile memories," Appl. Phys. lett., vol. 87, no. 20, 2005.
[29] D. Von Nordheim, S. Hahne, and B. Ploss, "Polarisation readout and determination of Landau parameters of PVDF-TrFE thin films from dielectric nonlinearities," Ferroelectrics, vol. 453, no. 1, pp. 122-126, 2013.
[30] B. Ploss, "Dielectric nonlinearity of PVDF−TrFE copolymer," Polymer, vol. 41, pp. 6087–6093, 2000.
[31] H. F. Wong et al., "Enhanced tunability of electrical and magnetic properties in (La,Sr)MnO_3 thin films via field-assisted oxygen vacancy modulation," Solid State Electron., vol. 138, pp. 56-61, 2017.
[32] H. F. Wong et al., "Modulating magnetism in ferroelectric polymer-gated perovskite manganite films with moderate gate pulse chains," ACS Appl. Mater. Interfaces, vol. 12, no. 50, pp. 56541-56548, Dec 16 2020.
[33] P. K. Muduli and R. C. Budhani, "Tailoring exchange bias in half-metallic $La_{2/3}Sr_{1/3}MnO_3$ thin films for spin valve applications," Appl. Phys. Lett., vol. 94, no. 20, 2009.
[34] P. K. Muduli and R. C. Budhani, "Tunneling magnetoresistance in spin valves exchange biased with metallic antiferromagnet $La_{0.45}Sr_{0.55}MnO_3$, " J. App. Phys. vol. 106, no. 10, 2009.
[35] D. Weber, R. Vőfély, Y. Chen, Y. Mourzina, and U. Poppe, "Variable resistor made by repeated steps of epitaxial deposition and lithographic structuring of oxide layers by using wet chemical etchants," Thin Solid Films, vol. 533, pp. 43-47, 2013.
[36] C. W. Leung and M. G. Blamire, "Interaction between ferromagnetic/antiferromagnetic systems across a common antiferromagnetic spacer," J. Appl. Phys., vol. 94, no. 11, pp. 7373-7375, 2003.
[37] J. Hemberger et al., "Structural, magnetic, and electrical properties of single-crystalline$La_{1-x}Sr_xMnO_3$ ($0.4<x<0.85$)," Phys. Rev. B, vol. 66, no. 9, 2002.
[38] Y. Moritomo, T. Akimoto, A. Nakamura, K. Ohoyama, and M. Ohashi, "Antiferromagnetic metallic state in the heavily doped region of perovskite manganites," Phys. Rev. B, vol. 58, pp. 5544-5549, 1998.
[39] C. Aruta et al., "Strain induced x-ray absorption linear dichroism in $La_{0.7}Sr_{0.3}MnO_3$ thin films," Phys. Rev. B, vol. 73, no. 23, 2006.
[40] "http://www.thermo.com.cn/Resources/201411/2412740468.pdf."
[41] H. W. Nesbitt and D. Banerjee, "Interpretation of XPS Mn(2p) spectra of Mn oxyhydroxides and constraints on the mechanism of MnO_2 precipitation," American Mineralogist, vol. 83, pp. 305–315, 1998.
[42] R. Pan, "Surface valence states of Mn ions and magnetic properties of $La_{0.67}Sr_{0.33}MnO_3$ films," Int. J. Mater. Sci. Appl., vol. 5, no. 5, 2016.
[43] J. Zhao et al., "Oxygen vacancy induced electronic structure variation in the $La_{0.2}Sr_{0.8}MnO_3$ thin film," AIP Adv., vol. 9, no. 5, 2019.
[44] X. Ke, M. S. Rzchowskia, L. J. Belenky, and C. B. Eom, "Positive exchange bias in ferromagnetic $La_{0.67}Sr_{0.33}MnO_3/SrRuO_3$ bilayers," Appl. Phys. lett., vol. 84, p. 5458, 2004.
[45] X. Zhao et al., "Exchange bias effect in epitaxial $La_{0.35}Sr_{0.65}MnO_3$/La0.7$Sr_{0.3}MnO_3$ bilayers: Impact of antiferromagnet growth conditions," Vacuum, vol. 175, 2020.
[46] C. Leighton, M. Song, J. Nogués, M. C. Cyrille, and I. K. Schuller, "Using magnetoresistance to probe reversal asymmetry in exchange biased bilayers," Journal of Applied Physics, vol. 88, no. 1, pp. 344-347, 2000.
[47] J. McCord, R. Schäfer, R. Mattheis, and K. U. Barholz, "Kerr observations of asymmetric magnetization reversal processes in CoFe/IrMn bilayer systems," Journal of Applied Physics, vol. 93, no. 9, pp. 5491-5497, 2003.

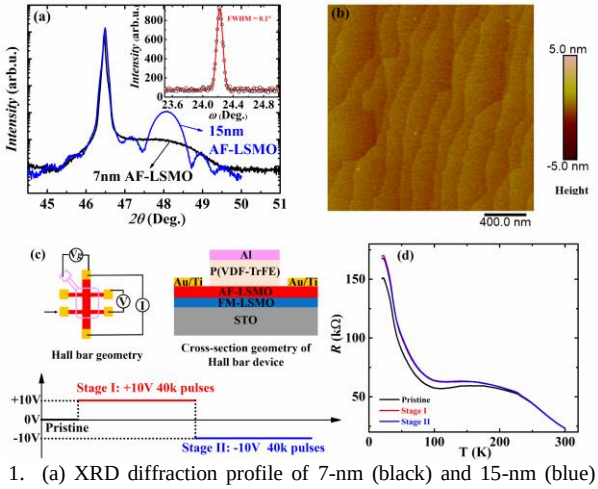

Fig. 1. (a) XRD diffraction profile of 7-nm (black) and 15-nm (blue) AF-LSMO thin films. Inset: rocking curve for 7-nm AF-LSMO at (002) peak. (b) AFM image of as-deposited 7-nm AF-LSMO film. (c) Schematic illustration of the planar view of Hall bar geometry (top left), cross-section geometry of Hall bar device (top right, note that single-layer AF-LSMO device has the same geometry just without the existence of FM-LSMO in the caption.) and pulsing protocol (bottom). (d) R-T plots of 7-nm AF-LSMO device for pristine, stage I, and stage II.

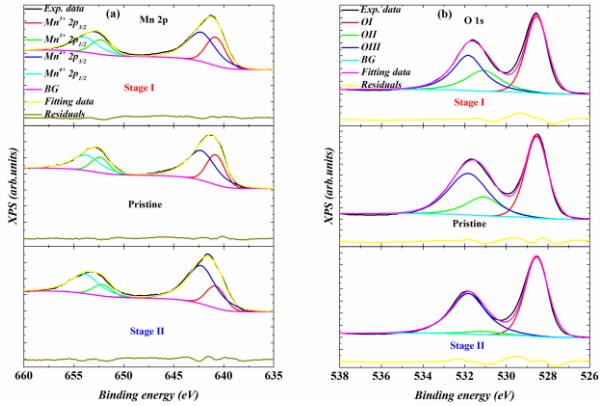

Fig. 2. XPS spectra of 7-nm AF-LSMO for pristine, stage I and stage II. (a) Mn 2p core-level spectra. (b) O 1s core-level spectra.

TABLE I Binding energies of Mn $2p_{3/2}$, Mn^{4+} ratio, OI and OII ratio of pristine, stage I and stage II

	Stage I	Pristine	Stage II
Binding energy of Mn $2p_{3/2}$ (eV)	641.3 ± 0.1	641.5 ± 0.1	641.6 ± 0.1
Mn^{4+} (%)	62.64 ± 1.8	64.2 ± 2.3	75.02 ± 2.9
OI (%)	46.03 ± 2.4	43.65 ± 2.9	52.47 ± 3.5
OII (%)	20.98 ± 2.7	16.46 ± 3.1	3.52 ± 3.7

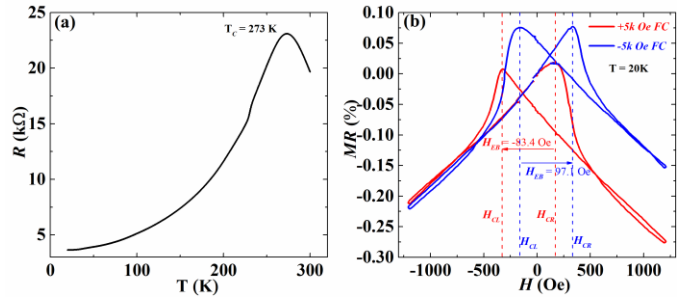

Fig. 3. (a) R-T plot of the bilayer device in pristine state. (d) MR curves of the bilayer device for pristine state at 20 K for +5k Oe and -5k Oe FC.

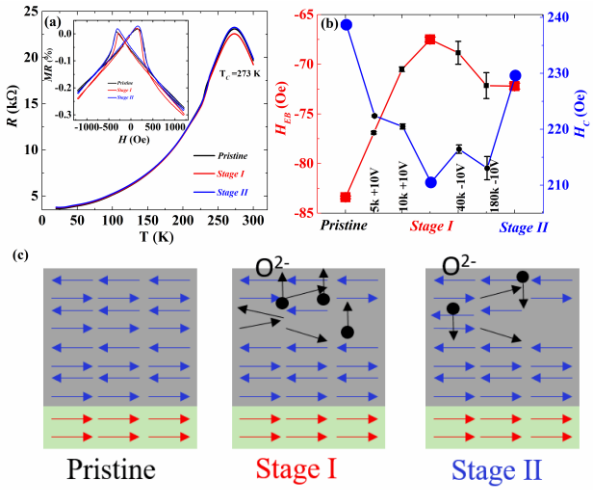

Fig. 4. (a) RT plots of AF-LSMO/FM-LSMO bilayer at different pulsing states. Inset: MR curves of different pulsing states at 20K. (b) The evolution of extracted H_C and H_{EB} at 20K. Note that more data points (solid black) are also recorded during the pulsing process. (c) Schematic illustration showing the relation between oxygen vacancy and spin disorder in the AF-LSMO layer.